Published in final edited form as:
Sci Transl Med. 2014 December 10; 6(266): 266ra173. doi:10.1126/scitranslmed.3010798.

White matter changes linked to visual recovery after nerve decompression

David A. Paul[1,2], **Elon Gaffin-Cahn**[1], **Eric B. Hintz**[1,3], **Giscard J. Adeclat**[4], **Tong Zhu**[5], **Zoë R. Williams**[6], **G. Edward Vates**[3], and **Bradford Z. Mahon**[1,3,7]

[1]Department of Brain and Cognitive Sciences, University of Rochester

[2]Department of Neurobiology and Anatomy, University of Rochester School of Medicine

[3]Department of Neurosurgery, University of Rochester School of Medicine

[4]Department of Neuroscience, University of Rochester

[5]Department of Radiation Oncology, University of Michigan Medical Center

[6]Department of Ophthalmology, University of Rochester School of Medicine

[7]Center for Visual Science, University of Rochester

Abstract

The relationship between the integrity of white matter tracts and cortical function in the human brain remains poorly understood. Here we use a model of reversible white matter injury, compression of the optic chiasm by tumors of the pituitary gland, to study the structural and functional changes that attend spontaneous recovery of cortical function and visual abilities after surgical tumor removal and subsequent decompression of the nerves. We show that compression of the optic chiasm leads to demyelination of the optic tracts, which reverses as quickly as 4 weeks after nerve decompression. Furthermore, variability across patients in the severity of demyelination in the optic tracts predicts visual ability and functional activity in early cortical visual areas, and pre-operative measurements of myelination in the optic tracts predicts the magnitude of visual recovery after surgery. These data indicate that rapid regeneration of myelin in the human brain is a significant component of the normalization of cortical activity, and ultimately the recovery of sensory and cognitive function, after nerve decompression. More generally, our findings demonstrate the utility of diffusion tensor imaging as an *in vivo* measure of myelination in the human brain.

Corresponding Author Bradford Z. Mahon Department of Brain and Cognitive Sciences Meliora Hall University of Rochester Rochester, NY 14627-0268, USA. mahon@rcbi.rochester.edu.

Author Contributions: D.A.P. planned and carried out the experiments, analyzed the data, generated the figures, and wrote the manuscript. E.G.C. and G.J.A. carried out the fMRI and psychophysical experiments, respectively, and analyzed the respective data. E.B.H, T.Z., Z.R.W, and G.E.V. planned the experiments and contributed to preparation of the manuscript. T.Z. also assisted with the analysis of the DTI data and G.E.V. performed all of the trans-sphenoidal pituitary tumor resections. B.Z.M. planned the experiments, analyzed the data, and wrote the manuscript.

Competing Interests: The authors do not have any competing interests.

Keywords

visual recovery; neural plasticity; myelin regeneration; secondary white matter injury; diffusion tensor imaging; functional magnetic resonance imaging; optic tracts; chiasmatic compression; pituitary tumor

Introduction

Delayed axonal degeneration (1, 2) describes a process of slow white matter injury that, if left unchecked, culminates in neuronal cell death. Despite the ubiquity of delayed axonal degeneration in humans, its impact on cortical function and cognitive performance is poorly understood. This is because delayed axonal degeneration is mediated by diffuse patterns of dysfunction in neuro-glial biology, including demyelination (3), impaired axonal transport (4), and glutamate excitotoxicity (5), and white matter tracts with transparent function are difficult to isolate in the human brain. Consequently, we do not have prognostic biomarkers that are able to predict whether cortical activation and cognitive function will recover to normal levels after white matter injury. Here we demonstrate the utility of a specific disease model – compression of the retinofugal nerve fibers by large pituitary tumors (6) – to characterize the relations between structural integrity of specific white matter tracts, cortical function, and visual abilities. Figure 1 demonstrates the normal morphology of the pituitary gland and its placement relative to the optic chiasm, and also shows several examples of pituitary tumors compressing the optic chiasm. Patients with large pituitary tumors often experience a characteristic loss of vision in the temporal hemi-fields and decreased contrast sensitivity (6, 7) due to selective compression of retinofugal fibers at the level of the optic chiasm (8). Surgical removal of the tumor and thus decompression of the optic chiasm is the most common treatment approach (9), with most patients (i.e., 80-90%) experiencing some level of visual recovery after surgery. There is, however, substantial patient-to-patient variability in both the initial distribution of visual impairments across the visual field, and the degree of recovery, which cannot be explained by tumor size (10), patient age (11), or pre-operative visual exam (12).

Past research suggests that demyelination contributes to delayed axonal degeneration after optic nerve compression (13, 14), although it is not clear how those processes alter early visual cortex function during the injured state and ultimately resolve to restore visual ability. One view is that improvement of secondary processes such as microtubule reorganization, axonal swelling, and ion channel permeability is responsible for early visual recovery (14, 15). Another view is that remyelination plays a significant role in supporting rapid recovery of visual abilities (13). An important observation in animal models is that partial remyelination can occur in as little as 2 to 4 weeks after a demyelinating event (16). However, it is not clear if remyelination occurs within the same time frame in the human brain, and if so, whether remyelination in the optic tracts is related to striate cortex function and ultimately the recovery of visual ability. While the use of fMRI and psychophysics to study the primate visual system is well established (17-22), there is only one study on pituitary tumor patients using fMRI – a case study, documenting both transient loss of visual ability and disruption of striate cortex (V1) activity after pituitary tumor compression (23).

Critically, that study was able to show that the pattern and magnitude of early visual cortex activation was directly related to the degree of visual field recovery, indicating a direct relationship between the re-afferentation of early visual cortex and visual abilities in patients undergoing removal of pituitary tumors.

Here we study delayed axonal degeneration using diffusion tensor imaging measurements made in cross-section along the length of the optic tracts from the chiasm to the lateral geniculate nucleus (LGN). We calculate diffusion along both the principal (Axial Diffusivity: AD) and perpendicular (Radial Diffusivity: RD) axes. The average of these two measures estimates total diffusion in all directions (Mean Diffusivity: MD), and the weighted variance (Fractional Anisotropy: FA) provides a measure of how strongly diffusion occurs in the principal direction (24). Previous work in the mouse optic nerve shows that decreased labeling of Myelin Basic Protein after retinal ischemia is associated with an increase in radial diffusivity (25). Thus, radial diffusivity may be used as an *in vivo* proxy for myelin integrity. Specifically, an increase in radial diffusivity that is disproportionate to changes in axial diffusivity is the signature of a breakdown in the myelin sheath (26-27). Using radial diffusivity as an *in vivo* measure of myelin integrity before and after surgical decompression of the optic chiasm, we show that i) remyelination occurs in the human optic tract within 4 weeks of surgical decompression of retinofugal fibers, ii) the degree of myelination of the optic tract is linked to normalization of retinotopic cortical function and visual abilities across patients, and iii) preoperative DTI measurements of myelination predict substantial variability in visual recovery across patients.

Results

We studied nine patients with compressive pituitary tumors before and after surgical tumor removal, as well as five patients with non-compressive pituitary tumors, and nine healthy control participants. Patients were tested with DTI, fMRI and psychophysics both before and after surgery, and all post-surgery testing occurred within 4 weeks of surgery. Non-compressive control patients completed the same battery of tests, but only before surgery. All controls completed DTI and visual psychophysics (see Materials and Methods, and Supplemental Materials for details).

Visual Psychophysics

Visual Field Mapping—Patients with compressive pituitary tumors demonstrated severe visual field deficits before surgery, primarily in the temporal hemi-fields. Within four weeks of surgery, visual fields dramatically improved for 71.4% of all hemi-fields tested, consistent with previous research (11). This is illustrated in Fig. 2A-C. Two key findings emerged from the visual field data: **i)** compared with all other participant groups, compressive pituitary tumor patients exhibited significantly reduced visual fields ($M = 0.629 \pm 0.0785$, significant at Bonferroni corrected levels, $p < 0.0083$), which dramatically recovered after surgery ($M = 0.881 \pm 0.0315$, $p < 0.006$), and **ii)** visual fields in participants with non-compressive pituitary tumors were not significantly different from healthy controls ($p = 0.993$).

Contrast Sensitivity—Compared with all other participant groups, individuals with compressive pituitary tumors (before surgery) exhibited decreased contrast sensitivity thresholds at all spatial frequencies tested (temporally stable stimuli, see Figs 2D-F; see Materials and Methods, and Supplemental Materials for details). Figure 2E displays the average full contrast sensitivity function for each participant group. We quantified the area under the log contrast sensitivity function (AULCSF) (21), weighted for each hemi-field as was done for visual fields (see Supp. Fig. S1). Analysis of AULCSF (see Fig. 2F) confirmed that patients with compressive pituitary tumors exhibited reduced contrast sensitivity ($M = 1.021 \pm 0.122$), significant at Bonferroni corrected levels, compared to healthy control participants ($M = 1.80 \pm 0.0765$, $p < 0.003$, and compared to non-compressive pituitary tumor patients, $M = 1.640 \pm 0.0957$, $p < 0.0015$). In contrast to the dramatic post-operative improvements observed for visual fields, surgical decompression led to only moderate recovery of contrast sensitivity. Following surgical decompression of the optic chiasm, 62.5% of hemi-fields showed increased contrast sensitivity 2-4 weeks after decompression. Contrast sensitivity for non-compressive pituitary tumor patients was numerically lower, but not significantly different from control levels ($p = 0.882$).

Diffusion Tensor Imaging

Figure 3 shows the diffusion measurements within each segment of the optic tract for patients and controls (see Materials and Methods and Supplemental Materials for all details of analyses). The threshold for significant findings was set at the Bonferroni corrected alpha level of $p < 0.0083$. The key finding is that increased radial diffusivity, computed across all segments in both optic tracts (Mean = $1.38\times10^{-3}mm^2/s\pm1$ STD = 0.048×10^{-3}) was the primary pathologic change in the pre-operative period for compressive pituitary tumor patients compared with healthy controls ($1.05\times10^{-3}mm^2/s\pm0.24\times10^{-3}$, significant at a Bonferroni corrected $p < 0.0083$). Increased pre-operative radial diffusivity in compressive pituitary tumor patients contributed to the observed changes in the other diffusion measurements, including reduced fractional anisotropy (0.24±0.004) and increased mean diffusivity ($1.57\times10^{-3}mm^2/s\pm0.054\times10^{-3}$; non-compressive tumor patients: FA 0.345±0.09; MD $1.21\times10^{-3}mm^2/s\pm 0.26\times10^{-3}$; healthy controls: FA 0.35±0.08; MD $1.30\times10^{-3}mm^2/s \pm0.26\times10^{-3}$; comparing compressive patients to controls, all ps < 0.0083). However, and critically, diffusion along the principal axis (axial diffusivity) of the optic tracts was not significantly different in compressive patients ($1.96\times10^{-3}mm^2/s\pm0.069\times10^{-3}$) compared to healthy controls ($1.80\times10^{-3}mm^2/s\pm0.20\times10^{3}$; p=0.87).

These data demonstrate a uniform pattern of increased radial diffusivity with spared diffusion along the principal axis in compressive pituitary tumor patients. This is in agreement with previous histological work in animal models that showed myelin disruption after axonal compression (13, 14), as well as combined DTI-histologic studies of isolated and reversible demyelinating lesions in mice (26). Individuals with non-compressive tumors (i.e., patient controls) demonstrated patterns of diffusion measurements that were equivalent to healthy control participants, indicating that the demyelination observed in the critical patients was directly tied to the tumor compression.

After surgery, thirteen of fourteen optic tracts in compressive pituitary tumor patients showed normalization in fractional anisotropy, mean diffusivity and radial diffusivity (refer to *Supp. Fig. S7* for a outlier analysis of the one tract that did not recover). A numerically (but statistically non-significant) trend was observed for axial diffusivity, in which ten of fourteen optic tracts demonstrated reduced axial diffusivity after surgery. While the diffusion indices largely resolved during the early phase of recovery (within 1 month after surgery), they did not fully return to healthy control values. Fig. 3 shows that anterior and posterior optic tract segments are more likely to demonstrate rapidly improved diffusion indices (see *Supp. Table S1* for a complete list of all diffusion indices in both the right and left optic tracts of all participants enrolled in the study).

Relation between myelination of the optic tracts and visual ability

We then tested whether variability across patients in myelination of the optic tracts, as measured with radial diffusivity, predicted visual abilities. This analysis is illustrated in Fig. 4 using a matrix of Pearson's Rho values for the correlation across patients between DTI indices in each optic tract segment and visual field performance (Fig. 4A) and contrast sensitivity (Fig. 4B). Higher levels of fractional anisotropy were associated with better visual abilities (positive Rho values), whereas higher levels of mean diffusivity and radial diffusivity were associated with worse visual abilities (negative Rho values). Importantly, there was little, if any, relationship between axial diffusivity and visual abilities. This pattern indicates that the key microstructural property in the optic tracts that is related to visual performance is the level of myelination. This also means that the relationships between visual abilities and mean diffusivity and fractional anisotropy were secondary to variability in radial diffusivity.

In order to evaluate whether the observed relationship between radial diffusivity and visual abilities was in fact driven by surgical decompression of the optic chiasm, we correlated the change in diffusivity indices with the change in visual abilities, for the subset of patients with compressive tumors in whom we had both pre- and post-operative DTI and visual fields data (n = 6). This analysis computed difference scores (post-operative minus pre-operative) across each segment of the optic tract for every subject, for the four DTI measures, as well as the post minus pre-operative difference in visual abilities. The resulting r-values (Fig 4D) relating DTI indices to visual abilities, averaged over all segments of the optic tract, confirmed the pattern observed in the cross sectional analyses. There was a relationship between radial diffusivity and visual fields (average $r = -0.62$, $p < .05$), and a weaker pattern for axial diffusivity (average $r = -0.52$, $p = .09$). There were also significant relationships between fractional anisotropy (average $r = 0.71$, $p < .05$) as well as mean diffusivity (average $r = 0.59$, $p < .05$) and visual fields. Finally, the relation between radial diffusivity and visual abilities was stronger than the relation between axial diffusivity and visual abilities (ttest, two-tailed, over fisher-transformed r-values for all segments in the optic tract: $t_{11} = 2.56$, $p < .05$). The same dissociation between radial and axial diffusivity was present when the analysis was repeated over fisher-transformed spearman rank-ordered correlation coefficients, ruling out a contribution from outlier data points ($t_{11} = 2.56$, $p < .05$).

In summary, regardless of whether the relationship between diffusion indices and visual abilities is carried out in a cross-sectional manner (Fig 4A-C) or within-patient in a longitudinal manner (Fig 4D), radial diffusivity explains more variance in visual abilities than does axial diffusivity.

Relation between diffusivity indices in the optic tracts and cortical retinotopic activity

If the degree of myelination in the optic tracts and visual abilities is in fact specifically related to the cascade of pathologies induced by compression of the early visual system, there should also be a relation between diffusion indices and the pattern of retinotopic activation in early visual areas. Fig. 5A displays retinotopic cortical activity in the right occipital lobe of a representative compressive pituitary tumor patient before and after surgery. Those data represent a replication of the findings of Chouinard and colleagues (23). Our principal interest was not in whether there was deformation of the retinotopic map (28, 29), but to use fMRI signal reproducibility in early visual areas as an objective and implicit measure of visual function. Thus, the fidelity of retinotopic preferences was calculated using linear correlation over multi-voxel patterns (30). This analysis correlated voxel-wise patterns, over beta values coding retinotopic preferences, between even and odd revolutions of the wedge within a run of polar angle mapping (for details see Materials and Methods, and *Supp. Fig. S5*). In order to ensure that we could replicate the findings of Chouinard and colleagues (23) using this novel approach, we correlated the variability in the resulting r-values across participants (by quadrant) to visual field maps (for the respective quadrants)—the results, indicated a relationship between visual fields and fMRI signal reproducibility ($r = 0.66$, $p < 0.01$). That relationship both extends the observations of Chouinard and colleagues (23) to an across-subject analysis, and validates this approach for using BOLD signal in striate cortex as an implicit measure of visual function.

We then tested whether variability across patients in fMRI signal reproducibility was related to variability in diffusivity indices, for each segment of the optic tract. As shown in Fig. 5C, mean diffusivity, axial diffusivity and radial diffusivity were all strongly predictive of fMRI signal reproducibility – with increased diffusivity values corresponding to decreased retinotopic activation. These data reveal an important dissociation: both axial diffusivity and radial diffusivity are related to fMRI signal reproducibility in striate cortex (Fig 5C), and fMRI signal reproducibility in striate cortex is related to visual ability (Fig 5B); however, only radial diffusivity is directly related to visual ability (Fig 4). This dissociation confirms that axial diffusivity and radial diffusivity are indexing different, and functionally relevant properties of the nerve fibers.

Pre-surgical DTI predicts visual recovery

Given the tight relationship between diffusion measurements of the optic tracts and visual abilities across the group of patients, a question of great clinical significance is whether it is possible to predict the degree of visual recovery (i.e., post-operative minus pre-operative visual fields) based only on pre-operative DTI data. From our dataset, we had pre- and post-operative visual fields data as well as preoperative DTI data in 6 patients (i.e., 12 hemispheres). We took two approaches – linear correlation and support vector regression –

to test whether pre-operative diffusion indices predict the change in visual abilities (i.e. visual field performance) as a function of surgery.

In the first analysis, we correlated pre-operative diffusivity indices for each segment of the optic tract with the change in visual abilities, across participants. The resulting correlation coefficients, averaged across all segments of the optic tracts, indicated that pre-operative radial diffusivity was significantly related to improvement in visual abilities (average r ± SEM over tract segments, one-sample t-test over fisher transformed r-values: 0.24 ± .05, t_{11}= 4.7, p < .0006). The corresponding analysis for axial diffusivity indicated only a marginally significant relationship between pre-operative axial diffusivity and change in visual abilities (r = 0.12 ± .06, t_{11} = 2.1, p = .06). Because both fractional anisotropy and mean diffusivity are derived from measures of radial and axial diffusivity, the corresponding analyses for those diffusivity indices were significant (FA: r = −0.27 ± .04, t_{11} = 6.8, p < .0001; MD: r = 0.21 ± .05, t_{11} = 3.9, p < .003). Finally, the relation between pre-operative radial diffusivity and visual improvement was stronger than the relation between pre-operative axial diffusivity and visual improvement (paired t-test over fisher transformed values, two tailed: t_{11} = 4.8, p < .0005).

In a second analysis, we used a machine-learning approach (Support Vector Regression—SVR) to test whether pre-operative variability in diffusivity indices along the segments of the optic tract predicted post-operative visual outcome. The feature vectors for support vector training and test consisted of the DTI indices along the segments of the optic tract, with each hemisphere in each patient constituting an observation. The significance of this approach, and what distinguishes it from the above approach based on linear correlation, is that SVR predicts a given hemisphere's visual outcome as a function of the preoperative DTI data for that hemisphere and support vectors that are trained on the other hemispheres in the dataset (i.e. jackknifed across all hemispheres in the dataset).

We evaluated the reliability of the trained support vectors in two ways. First, we computed the linear correlation between predicted visual abilities and observed visual abilities, and from that the explained variance (r-squared). This analysis indicated that pre-operative radial diffusivity predicted 49% of the variance in observed visual outcome (p < .05) while pre-operative axial diffusivity predicted 17% of the variance in observed visual outcome (p > .05). Second, we used a Monte-Carlo style permutation test in which, on each of 100,000 iterations, the training data were randomly shuffled, and each of 12 hemispheres individually tested (having trained the support vectors on the remaining 11 hemispheres; Figure 6B). These permutation tests generated null distributions of r-squared values (i.e., explained variance) for each of the four diffusivity indices. Plotted in each null distribution is the performance of the support vector regression model on un-shuffled data (i.e., from Figure 6A). The results of these permutations tests indicated that pre-operative radial diffusivity predicted visual recovery better than 98.7% of the null distribution (i.e., bootstrapped p < .014), while pre-operative axial diffusivity predicted visual recovery better than 81.5% of the null distribution (bootstrapped p = .18). Preoperative fractional anisotropy predicted visual recovery better than 98.3% of the null distribution (bootstrapped p < .02), while preoperative mean diffusivity predicted visual recovery better than 93.2% of the null

distribution (bootstrapped p = .068; null distribution for fractional anisotropy and mean diffusivity not shown in Figure 6).

Taken together, there is a dissociation between the ability of pre-operative radial and axial diffusivity to predict visual recovery: pre-operative radial diffusivity is significantly correlated across patients with the change in visual abilities, and predicts a substantial portion of variance in visual outcome (49%), while axial diffusivity is at best weakly correlated with the change in visual abilities and predicts only a modest (and non-significant) amount of variance in visual outcome (17%).

Discussion

Compression of the optic chiasm by large pituitary tumors is a disease model that permits *in vivo* and longitudinal analysis of the effects of nerve crush injury on white matter tracts in the human brain. Surgical removal of the tumors and subsequent decompression of the early visual pathway has long been known to be associated with a staged return of visual abilities. Here we found that demyelination of the optic tracts is a key aspect of white matter injury caused by pressure block injury in the brain, and that substantial remyelination occurs within four weeks of surgical decompression. Furthermore, the degree of myelination across patients is directly related to visual ability, and pre-operative measurements of myelination in the optic tracts predict nearly half of the variance in visual recovery. These findings demonstrate the speed of remyelinating processes in the central nervous system in humans and show that those regenerative processes are the driving force behind the rapid recovery of visual abilities that follow surgical decompression of the early visual pathway. These data also indicate that pre-operative measurements provide a basis for predicting a substantial portion of variability in visual recovery, and more generally, support the use of radial diffusivity as an *in vivo* measure of myelination in the human brain.

As previously discussed, an important precedent for the current investigation are combined DTI-histological studies in animal models that collectively support the connection between radial diffusivity and myelin integrity across a wide range of experimentally induced pathologies, including retinal ischemia (25), cuprizone mediated demyelination (26), transgenic shiverer mice (27), dorsal root axotomy (31), and wallerian degeneration (32). An increase in radial diffusivity that is both disproportionate to changes in axial diffusivity and consistent with the direction of the principal eigenvector (33) is an indication of decreased myelination. Similarly, a reduction in radial diffusivity independent of changes in axial diffusivity (26) is associated with remyelination. This has been demonstrated with decreased radial diffusivity following injection of human oligodendrocyte precursor stem cells into patients with a rare hypomyelinating genetic disorder, Pelizaeus-Merzbacher disease (34). Importantly, we were able to ensure the uniformity of the principal eigenvector across subjects by implementing a probabilistic tractography approach (see Materials and Methods, Supp. Materials for details). It is also important to note that an increase in radial diffusivity pre-operatively, followed by a decrease in axial diffusivity would be suggestive of severe axonal damage, often expressed as either wallerian degeneration or late stage tissue ischemia (25). However, because in the present study axial diffusivity remained stable across the cohort of compressive pituitary tumor patients, it is not likely that wallerian degeneration or

tissue ischemia played a significant role in these patients with pressure block injury to the early visual pathways. Rapid remyelination from zero to four weeks after nerve decompression satisfies both the anatomic and physiologic requirements of a functionally significant reduction in radial diffusivity (4, 35). This conclusion is consistent with the findings of Naismith and colleagues (2010), who found that radial diffusivity in the optic nerves strongly correlates with both VEP conduction velocity (an indirect measure of myelination), as well as severity of vision loss at approximately six months after a remote episode of optic neuritis (36).

To date, one of the difficulties associated with the diagnosis of secondary white matter injury, and thus an important obstacle for developing prognostic indicators and measuring the efficacy of novel therapeutics, is that it has not been clear what combination of DTI indices should be tested. Patients with pituitary tumors offer a new model for understanding both the process of spontaneous remyelination in the human brain and the functional consequences of that remyelination, and therefore, provide new leverage on the development of biomarkers for secondary white matter injury. This is significant, because as noted above, there have been notable failures to predict the likelihood of visual recovery following decompression of retinofugal nerves: factors such as tumor size, duration of compression, severity of pre-surgical visual impairments, and age do not predict visual outcome (10-12). Previous neuro-ophthalmologic research on macroadenoma patients (15, 37) using pattern electroretinography (PERG), photopic negative response (PhNR) and retinal nerve fiber layer (RNFL) thickness has found that PERG is able to predict only failure of visual recovery (38), whereas post-operative PhNR and RNFL thickness significantly correlate with visual field outcomes at three to six months (15). However, PhNR and RNFL thickness do not increase during the early phase of visual recovery—i.e., within the time frame of the current study (15). Increased visual ability in the absence of a corresponding increase in RNFL and PhNR values during the early phase of recovery supports the notion that retinal ganglion cell health cannot be the complete story behind improved visual outcomes.

DTI presents several advantages over other available techniques, such as visual evoked potentials and OCT-based measurements of RNFL. First, we have established a role for radial diffusivity in the assessment of subtle structural changes to the visual system that cannot be measured using PhNR or RNFL. It should be noted though that there is likely to be a threshold or cut-off on the predictive utility of radial diffusivity, as is the case for RNFL, beyond which irreparable damage to the axons has occurred and visual recovery is not feasible. But importantly, this means that radial diffusivity provides a sensitive measure with which to assess subtle changes that may not be detectable with RNFL. Further studies relating diffusion measurements, particularly axial diffusivity, with RNFL in healthy individuals and across a broad range of ophthalmologic diseases are needed to establish the relation between diffusion indices and ganglion cell anatomy in the human visual pathways. Furthermore, combining RNFL, DTI and visual evoked potentials in longitudinal assessments of patients undergoing chiasmatic decompression offers a promising approach toward developing a comprehensive suite of noninvasive *in vivo* biomarkers for myelination with general application.

A second advantage of DTI over other approaches for assessing myelination of nerve fibers is that it provides a means to study the structural integrity of isolated white matter tracts, and even isolated segments of specific white matter tracts, independent of their function. This is important because while it is possible to study the function of the retinofugal nerve pathway (using retinotopic fMRI and visual psychophysics), this is often not feasible for major white matter pathways that link high-level cortical regions in the brain. With DTI, we have shown that it is possible to identify the diffusion related changes that lead to functional impairments prior to neuronal cell death, and to identify the structural changes that facilitate functional recovery. This offers a new means with which to directly measure the efficacy of novel therapies designed to promote the regeneration of myelin in the human brain (39).

Materials and Methods

Participant Recruitment

Patients were recruited as part of an ongoing pituitary tumor research study approved by the Research Subjects Review Board (RSRB) at the University of Rochester. Individuals diagnosed with a pituitary or para-sellar tumor without any confounding factors, including glaucoma, diabetic retinopathy, multiple sclerosis, stroke, or previous head trauma, between September 2012 and August 2013 are included in this study. Healthy controls (n = 9) were also recruited from the Rochester, NY community and underwent the same battery of DTI and psychophysical testing as the patient group. *Supp. Table S1* displays the demographic information for all study participants. All patients and healthy control subjects gave written informed consent (see Supp. Materials for additional participant information).

Assessment of Visual Psychophysics

Each participant was tested monocularly in both eyes, at a viewing distance of 50 cm (ViewSonic VX2265WM; resolution, 1680x1050; 120Hz; average background luminance, 166 cd/m^2). Fixation was monitored using an Eyelink 1000 EyeTracker. For visual field testing, high contrast letters were presented (one per trial) ten times the minimum size for recognition at different locations in the visual field (40), and participants verbally named the letters (see Fig. 2A). All letter stimuli were presented within 14° of a black fixation cross. Contrast sensitivity (CS) thresholds were measured using a Bayesian algorithm that allows fast estimation of the CS curve (21). Each hemi-field was tested for each eye using temporally stable stimuli (Gabor patches 3° in diameter) of varying spatial frequency, up to ten cycles per degree. Stimuli were presented 8° to either the right or left of a black fixation cross and participants were asked to judge whether the stimulus was oriented 45° to the right or left (see Fig. 2D for an example stimulus).

MRI Acquisition Parameters

All participants were scanned at the Rochester Center for Brain Imaging on a 3-Tesla Siemens MAGNETOM Trio scanner with a 32-channel head coil. High-resolution sagittal T1-weighted anatomical images were acquired at the start of each session with a MPRAGE pulse sequence (TR = 2530 ms, TE = 3.44 ms, flip angle = 7°, FOV = 256mm, matrix = 256×256, 1×1×1mm). DTI was acquired using a single shot echo-planar sequence (60 diffusion directions, TR/TE=8900/86 ms, b = 1000 s/mm^2, 70 slices with resolution of

2×2×2 mm, 10 non-diffusion weighted volumes). BOLD fMRI was obtained with an echo-planar imaging pulse sequence (TR = 2000 ms, TE = 30 ms, flip angle = 90°, FOV = 256mm, matrix 64×64, 30 sagittal left-to-right slices, iso-voxel size 4×4×4mm).

fMRI Stimulus Presentation

Cortical activation in early visual areas was elicited using a (clockwise) rotating wedge stimulus that subtended 21.6°, and consisted of a high contrast green- and red-checkerboard pattern that flickered at 5 Hz and scaled with eccentricity. The wedge completed one rotation in 64 seconds and made 8 clockwise rotations per functional run. Subjects were instructed to focus their gaze on a fixation cross located at the center of screen. Because of time limitations, it was possible to study only one eye in each participant (the other eye was patched). In all patients we used monocular performance on the visual field test prior to scanning to determine which eye had the most clearly compromised impairment that was specific to a region of the visual field.

Pre-processing of MRI data

DTI—Motion artifacts, eddy current distortions, and B0 distortions were reduced using the FMRIB software library (FSL 4.1.8, www.fmrib.ox.ac.uk/fsl) (41). Probability distributions of fiber direction at each voxel (up to 2/voxel) in the pre-processed DTI sets were calculated using Bayesian estimation of diffusion parameters (BEDPOSTX) in FSL. Additionally, each pre-processed DTI image was brain extracted using BET, prior to image registration. The first non-diffusion weighted (b=0) volume in each subject was then registered to the corresponding skull-stripped T1 weighted image and the MNI152 template using a correlation ratio cost function and 6 degrees of freedom to define transformation matrices between the spaces.

fMRI—The first two volumes of each run were discarded for signal equilibration. Preprocessing of fMRI data included slice time correction, 3D motion correction aligned to the first run, and high pass temporal filtering (>2 cycles/run) linear co-registration on a subject-by-subject basis to the deskulled T1 anatomical image, and conversion to standardized Talairach space. Preprocessing was performed using BrainVoyagerQX batched with custom scripts.

Data Analysis

DTI tractography—To isolate the optic tracts we used probabilistic tractography – a Bayesian method for calculating the probability density functions of white matter connections in the brain (42). Because of the extremely small cross-sectional area of the optic tracts (43), 5.1-11.3 mm^2 and neighboring antero-posterior tract groups, a single-voxel seed mask was used to generate the tract profile (See *Supp. Materials, Supp. Fig S3*).

Along Tract Statistics Algorithm: Various along-tract statistics algorithms have been used previously to study white matter changes during development and in disease (44, 45). Here, we use a novel approach loosely based on methods developed to analyze geospatial representations of river channels (46). Full details of this analysis can be found in the Supplemental Materials (See Supp. Fig S4).

Defining retinotopic information content in early visual cortex (fMRI)— Retinotopically responsive voxels were identified for each hemi-field separately, using phase-lag analysis (with the left- or the right-half of the checkerboard sweep, as is standard). Each run was analyzed separately, and retinotopically responsive voxels were determined as those voxels that met or surpassed a threshold of $r > .30$ and fell within the bounds of an occipital lobe mask. To define the strength of retinotopic response to the visual stimuli, we ran a fixed effects GLM (using a standard dual gamma HRF) for each run with predictors for each quadrant that excluded time points when the checkerboard stimulus was at the vertical or horizontal meridians, and separate predictors for even and odd revolutions of the wedge (i.e., 8 predictors per GLM). Refer to the supplemental materials and Supp. Fig S5 for details.

Statistics

All data are presented as means ± 1 standard deviation unless stated otherwise. The MATLAB software package was used for all statistical analyses and comparisons were Bonferroni corrected at $p < 0.05$ for significance. Details of the individual statistical tests are provided in the supplementary materials and methods section.

Supplementary Material

Refer to Web version on PubMed Central for supplementary material.

Acknowledgements

The authors are grateful to Anat Fintzi and Duje Tadin for their contributions to the development of the visual psychophysical tests, and to Tania Pasternak, Bill Merigan, and Peter Shrager for their comments on earlier drafts.

Funding: This research was supported by NINDS grant NS076176 to B.Z.M. and NEI core grant P30 EY001319 to the Center for Visual Science. D.A.P. was supported by a grant from the University of Rochester Clinical and Translational Science Institute (CTSI TL1 TR000096) and the American Association of Neurological Surgeons MSSRF.

References and Notes

1. Crowe MJ, Bresnahan JC, Shuman SL, Masters JN, Beattie MS. Apoptosis and delayed degeneration after spinal cord injury in rats and monkeys. Nat. Med. 1997; 3:73–76. [PubMed: 8986744]
2. Yoles E, Schwartz M. Degeneration of spared axons following partial white matter lesion: implications for optic nerve neuropathies. Exp. Neurol. 1998; 153:1–7. [PubMed: 9743562]
3. Totoiu MO, Keirstead HS. Spinal cord injury is accompanied by chronic progressive demyelination. Journal of Comparative Neurology. 2005; 486:373–383. [PubMed: 15846782]
4. Maxwell WL, Graham DI. Loss of axonal microtubules and neurofilaments after stretch-injury to guinea pig optic nerve fibers. J. Neurotrauma. 1997; 14:603–614. [PubMed: 9337123]
5. Park E, Velumian AA, Fehlings MG. The role of excitotoxicity in secondary mechanisms of spinal cord injury: a review with an emphasis on the implications for white matter degeneration. J. Neurotrauma. 2004; 21:754–774. [PubMed: 15253803]
6. Cushing H, Walker CB. Distortions of the visual fields in cases of brain tumor chiasmal lesions, with especial reference to bitemporal hemianopsia. Brain. 1915; 37:341–400.
7. Porciatti V, et al. Losses of hemifield contrast sensitivity in patients with pituitary adenoma and normal visual acuity and visual field. Clinical Neurophysiology. 1999; 110:876–886. [PubMed: 10400201]

8. Tassinari G, Marzi C, Lee B, Di Lollo V, Campara D. A possible selective impairment of magnocellular function in compression of the anterior visual pathways. Experimental Brain Research. 1999; 127:391–401. [PubMed: 10480274]
9. Ciric I, Mikhael M, Stafford T, Lawson L, Garces R. Transsphenoidal microsurgery of pituitary macroadenomas with long-term follow-up results. J. Neurosurgery. 1983; 59:395–401.
10. Tokumaru A, et al. Optic nerve hyperintensity on T2-weighted images among patients with pituitary macroadenoma: correlation with visual impairment. American journal of neuroradiology. 2006; 27:250–254. [PubMed: 16484385]
11. Gnanalingham KK, Bhattacharjee S, Pennington R, Ng J, Mendoza N. The time course of visual field recovery following transphenoidal surgery for pituitary adenomas: predictive factors for a good outcome. J. Neurol. Neurosurg. Psychiatry. 2005; 76:415–419. [PubMed: 15716538]
12. Chacko A, Babu K, Chandy M. Value of visual evoked potential monitoring during trans-sphenoidal pituitary surgery. British journal of neurosurgery. 1996; 10:275–278. [PubMed: 8799538]
13. Clifford-Jones RE, Landon DN, McDonald WI. Remyelination during optic nerve compression. Journal of the Neurological Sciences. 1980; 46:239–243. [PubMed: 7381514]
14. Cottee LJ, Daniel C, Loh WS, Harrison BM, Burke W. Remyelination and recovery of conduction in cat optic nerve after demyelination by pressure. Experimental Neurology. 2003; 184:865–877. [PubMed: 14769379]
15. Moon CH, Hwang SC, Ohn Y-H, Park TK. The Time Course of Visual Field Recovery and Changes of Retinal Ganglion Cells after Optic Chiasmal Decompression. Invest. Ophthalmol. Vis. Sci. 2011; 52:7966–7973. [PubMed: 21896856]
16. Sim FJ, Hinks GL, Franklin RJM. The re-expression of the homeodomain transcription factor Gtx during remyelination of experimentally induced demyelinating lesions in young and old rat brain. Neuroscience. 2000; 100:131–139. [PubMed: 10996464]
17. Engel SA, et al. fMRI of human visual cortex. Nature. 1994; 369:525. [PubMed: 8031403]
18. Engel SA, Glover GH, Wandell BA. Retinotopic organization in human visual cortex and the spatial precision of functional MRI. Cereb Cortex. 1997; 7:181–192. [PubMed: 9087826]
19. Jiang X, et al. Categorization training results in shape-and category-selective human neural plasticity. Neuron. 2007; 53:891–903. [PubMed: 17359923]
20. Konen CS, Behrmann M, Nishimura M, Kastner S. The functional neuroanatomy of object agnosia: a case study. Neuron. 2011; 71:49–60. [PubMed: 21745637]
21. Lesmes LA, Lu ZL, Baek J, Albright TD. Bayesian adaptive estimation of the contrast sensitivity function: the quick CSF method. J. Vis. 2010; 10:17, 1–21. [PubMed: 20377294]
22. Sereno MI, et al. Borders of multiple visual areas in humans revealed by functional magnetic resonance imaging. Science. 1995; 268:889–893. [PubMed: 7754376]
23. Chouinard PA, et al. Retinotopic organization of the visual cortex before and after decompression of the optic chiasm in a patient with pituitary macroadenoma. J. Neurosurgery. 2012; 117:218–224.
24. Basser PJ, Jones DK. Diffusion-tensor MRI: theory, experimental design and data analysis -a technical review. NMR Biomed. 2002; 15:456–467. [PubMed: 12489095]
25. Song SK, et al. Diffusion tensor imaging detects and differentiates axon and myelin degeneration in mouse optic nerve after retinal ischemia. Neuroimage. 2003; 20:1714–1722. [PubMed: 14642481]
26. Song S-K, et al. Demyelination increases radial diffusivity in corpus callosum of mouse brain. Neuroimage. 2005; 26:132–140. [PubMed: 15862213]
27. Song S-K, et al. Dysmyelination Revealed through MRI as Increased Radial (but Unchanged Axial) Diffusion of Water. Neuroimage. 2002; 17:1429–1436. [PubMed: 12414282]
28. Dilks DD, Serences JT, Rosenau BJ, Yantis S, McCloskey M. Human adult cortical reorganization and consequent visual distortion. J. Neurosci. 2007; 27:9585. [PubMed: 17804619]
29. Wandell BA, Smirnakis SM. Plasticity and stability of visual field maps in adult primary visual cortex. Nat Rev Neurosci. 2009; 10:873–884. [PubMed: 19904279]

30. Haxby JV, et al. Distributed and overlapping representations of faces and objects in ventral temporal cortex. Science. 2001; 293:2425–2430. [PubMed: 11577229]
31. Zhang J, et al. Diffusion tensor magnetic resonance imaging of Wallerian degeneration in rat spinal cord after dorsal root axotomy. J.Neurosci. 2009; 29:3160–3171. [PubMed: 19279253]
32. Qin W, et al. Wallerian degeneration in central nervous system: dynamic associations between diffusion indices and their underlying pathology. PLoS One. 2012; 7:e41441. [PubMed: 22829950]
33. Wheeler-Kingshott CA, Cercignani M. About “axial” and “radial” diffusivities. Magn. Reson. Med. 2009; 61:1255–1260. [PubMed: 19253405]
34. Gupta N, et al. Neural stem cell engraftment and myelination in the human brain. Science translational medicine. 2012; 4:155ra137.
35. Le Bihan D, et al. Diffusion tensor imaging: concepts and applications. J.Magn. Reson. Imaging. 2001; 13:534–546. [PubMed: 11276097]
36. Naismith RT, et al. Radial diffusivity in remote optic neuritis discriminates visual outcomes. Neurology. 2010; 74:1702–1710. [PubMed: 20498438]
37. Danesh-Meyer HV, et al. In vivo retinal nerve fiber layer thickness measured by optical coherence tomography predicts visual recovery after surgery for parachiasmal tumors. Invest. Ophthalmol. Vis. Sci. 2008; 49:1879–1885. [PubMed: 18263812]
38. Parmar DN, Sofat A, Bowman R, Bartlett JR, Holder GE. Visual prognostic value of the pattern electroretinogram in chiasmal compression. Br. J.Ophthalmol. 2000; 84:1024–1026. [PubMed: 10966958]
39. Franklin RJM, Ffrench-constant C. Remyelination in the CNS: from biology to therapy. Nature Reviews. Neuroscience. 2008; 9:839–855.
40. Anstis SM. A chart demonstrating variations in acuity with retinal position. Vision Res. 1974; 14:589–592. [PubMed: 4419807]
41. Smith SM, et al. Advances in functional and structural MR image analysis and implementation as FSL. Neuroimage. 2004; 23(Supplement 1):S208–S219. [PubMed: 15501092]
42. Behrens TEJ, Berg HJ, Jbabdi S, Rushworth MFS, Woolrich MW. Probabilistic diffusion tractography with multiple fibre orientations: What can we gain? Neuroimage. 2007; 34:144–155. [PubMed: 17070705]
43. Andrews TJ, Halpern SD, Purves D. Correlated size variations in human visual cortex, lateral geniculate nucleus, and optic tract. J. Neurosci. 1997; 17:2859–2868. [PubMed: 9092607]
44. Gong G, et al. Asymmetry analysis of cingulum based on scale-invariant parameterization by diffusion tensor imaging. Human Brain Mapping. 2005; 24:92–98. [PubMed: 15455461]
45. Yeatman JD, Dougherty RF, Myall NJ, Wandell BA, Feldman HM. Tract profiles of white matter properties: automating fiber-tract quantification. PLoS One. 2012; 7:e49790. [PubMed: 23166771]
46. Merwade V, Maidment D, Hodges B. Geospatial Representation of River Channels. Journal of Hydrologic Engineering. 2005; 10:243–251.
47. Kriegeskorte N, Simmons WK, Bellgowan PS, Baker CI. Circular analysis in systems neuroscience: the dangers of double dipping. Nat. Neuroscience. 2009; 12:535–540.
48. Dasenbrock HH, et al. Diffusion tensor imaging of the optic tracts in multiple sclerosis: association with retinal thinning and visual disability. J. Neuroimaging. 2011; 21:e41–e49. [PubMed: 20331501]
49. Brainard DH. The psychophysics toolbox. Spatial vision. 1997; 10:433–436. [PubMed: 9176952]
50. Pelli DG. The VideoToolbox software for visual psychophysics: Transforming numbers into movies. Spatial vision. 1997; 10:437–442. [PubMed: 9176953]
51. Kupfer C, Chumbley L, Downer J. d. C. Quantitative histology of optic nerve, optic tract and lateral geniculate nucleus of man. Journal of anatomy. 1967; 101:393–401. [PubMed: 6051727]

One Sentence Summary

Rapid remyelination is a major contributor to the normalization of function after nerve decompression in the human brain.

Highlights

- Rapid remyelination in the human brain shown *in vivo* using diffusion tensor MRI
- Reversible white matter injury reveals structure-function relationships in the adult human brain
- Structural plasticity of the optic tracts in adult humans
- Pre-operative DTI predicts post-operative visual recovery

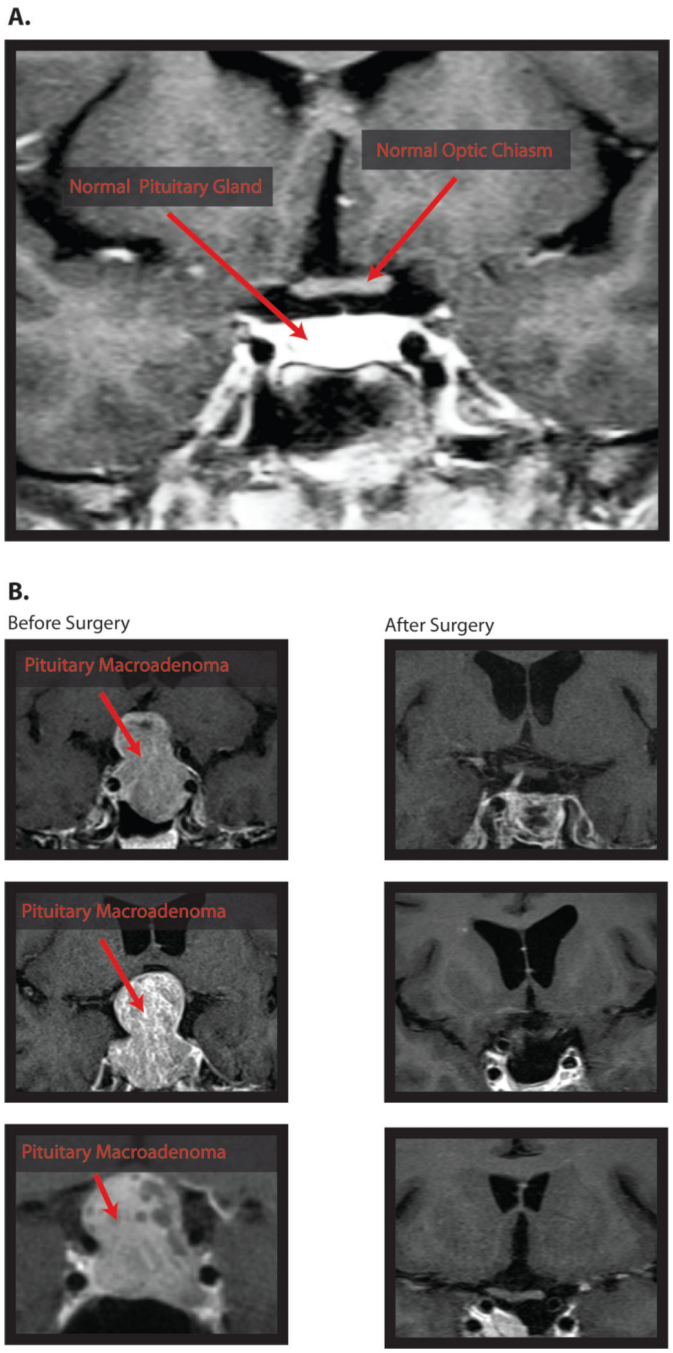

Figure 1. Pituitary macroadenomas

(A) A coronal T1-weighted MRI with contrast at the level of the optic chiasm in a healthy participant showing the normal morphology of the pituitary gland and it's relationship to the anterior visual pathway. **(B)** Coronal T1-MRIs with contrast for 3 compressive macroadenoma patients. In all three cases, the tumor displays significant suprasellar extension and consequent upward displacement of the optic chiasm.

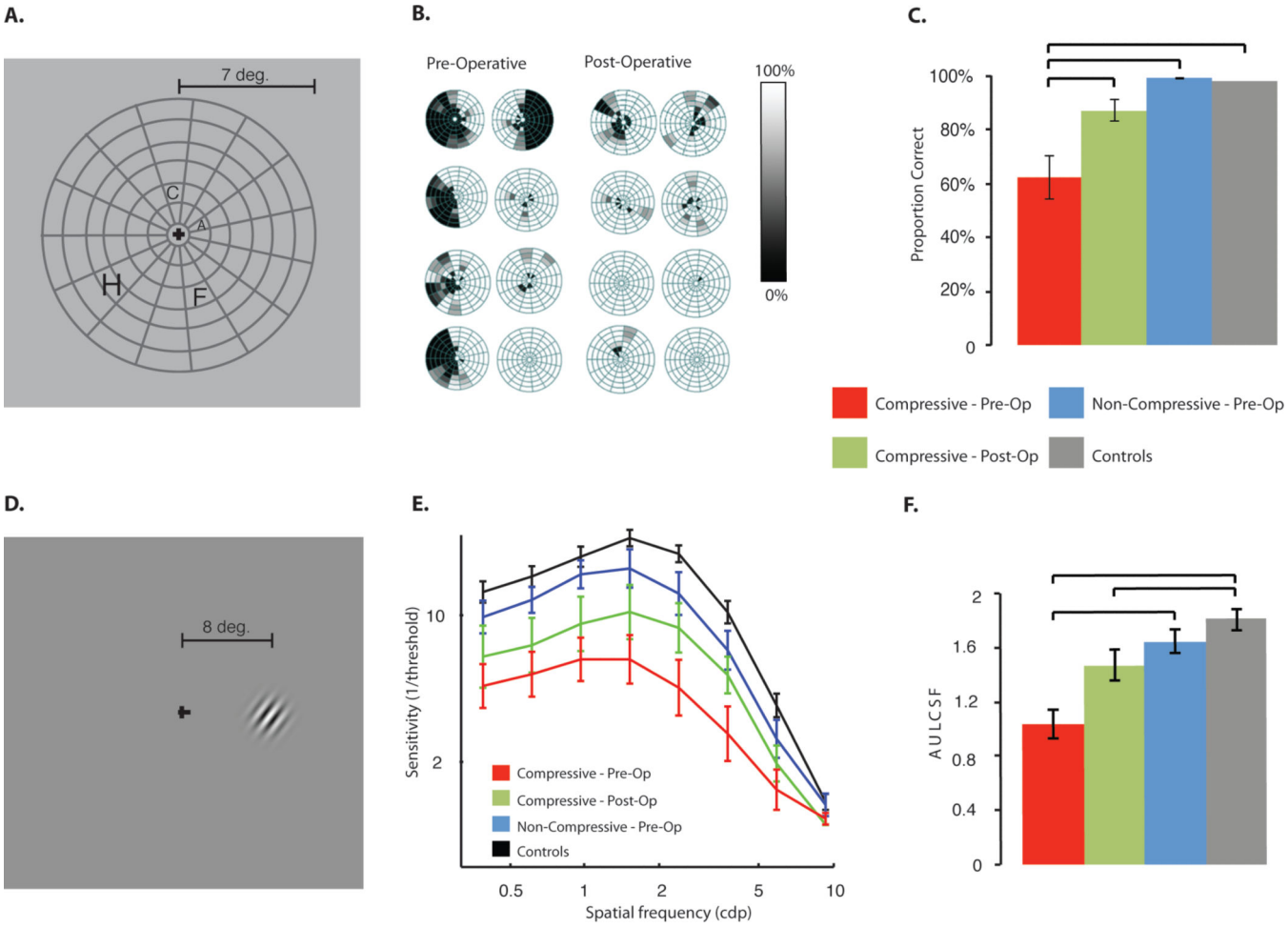

Figure 2. Visual psychophysics tests

All psychophysical tests were completed monocularly. Panels A-C show visual fields testing, while Panels D-F show contrast sensitivity. **(A)** Examples of stimuli used to assess visual fields. On each trial a single letter was presented. (**B)** Visual fields, represented as % correct letter identification, for a sample of compressive pituitary tumor patients, before and after surgery. The raw data were spatially (Gaussian) smoothed. (**C)** Visual fields were significantly reduced for pre-operative compressive pituitary tumor patients ($p < 0.0083$; Bonferroni corrected) and recovered with surgical tumor removal. Visual fields for non-compressive pituitary tumor patients were not different from healthy control participants. **(D)** Participants were tested using Gabor patches that orthogonally varied spatial frequency (up to 10 cpd) and contrast (stable stimuli, presented 8° to the right or left of fixation). (**E)** The mean contrast sensitivity function for each participant group is shown and the error bars represent standard error of the mean over subjects. (**F)** Contrast sensitivity, represented by the area under the log contrast sensitivity function (AULCSF, see Supp. Fig S2), was significantly reduced before surgery ($p < 0.0083$), but unlike visual fields, did not return to healthy control values after surgery (after surgery $p < 0.0083$). Non-compressive pituitary tumor patients were not significantly different than healthy control participants.

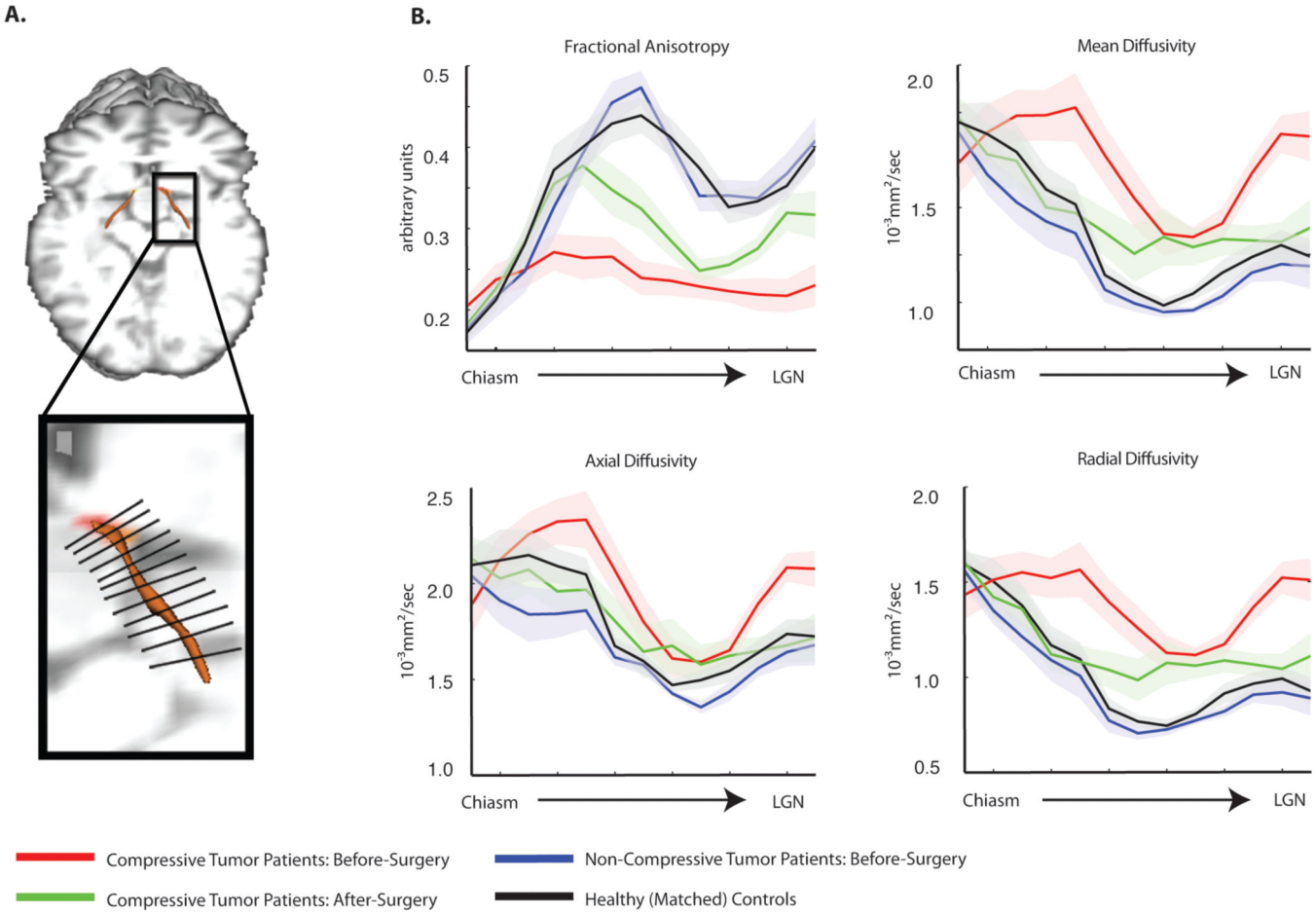

Figure 3. Along-tract analysis of diffusion indices

(A) Displayed is a schematic illustration of a segmented optic tract into thirteen equidistant bins from the chiasm to LGN using the along-tract statistics algorithm implemented in this study (for the basis of this approach, see Merwade et al., 2005; for all details, see *Supp. Materials and Fig. S4*). **(B)** Measures of diffusion (fractional anisotropy, mean diffusivity, axial diffusivity, and radial diffusivity) were extracted from each segment, for each participant, and are plotted by segment position within each group. The shaded region around each line represents the standard error of the mean (over participants). The consistent pattern of variability in diffusion measurements, for all participant groups, along the length of the optic tract results from the proximity of the optic tracts to major fiber bundles, particularly the corticospinal tracts. This observation is in line with previous studies of the optic tracts (49) and other white matter fiber bundles (44).

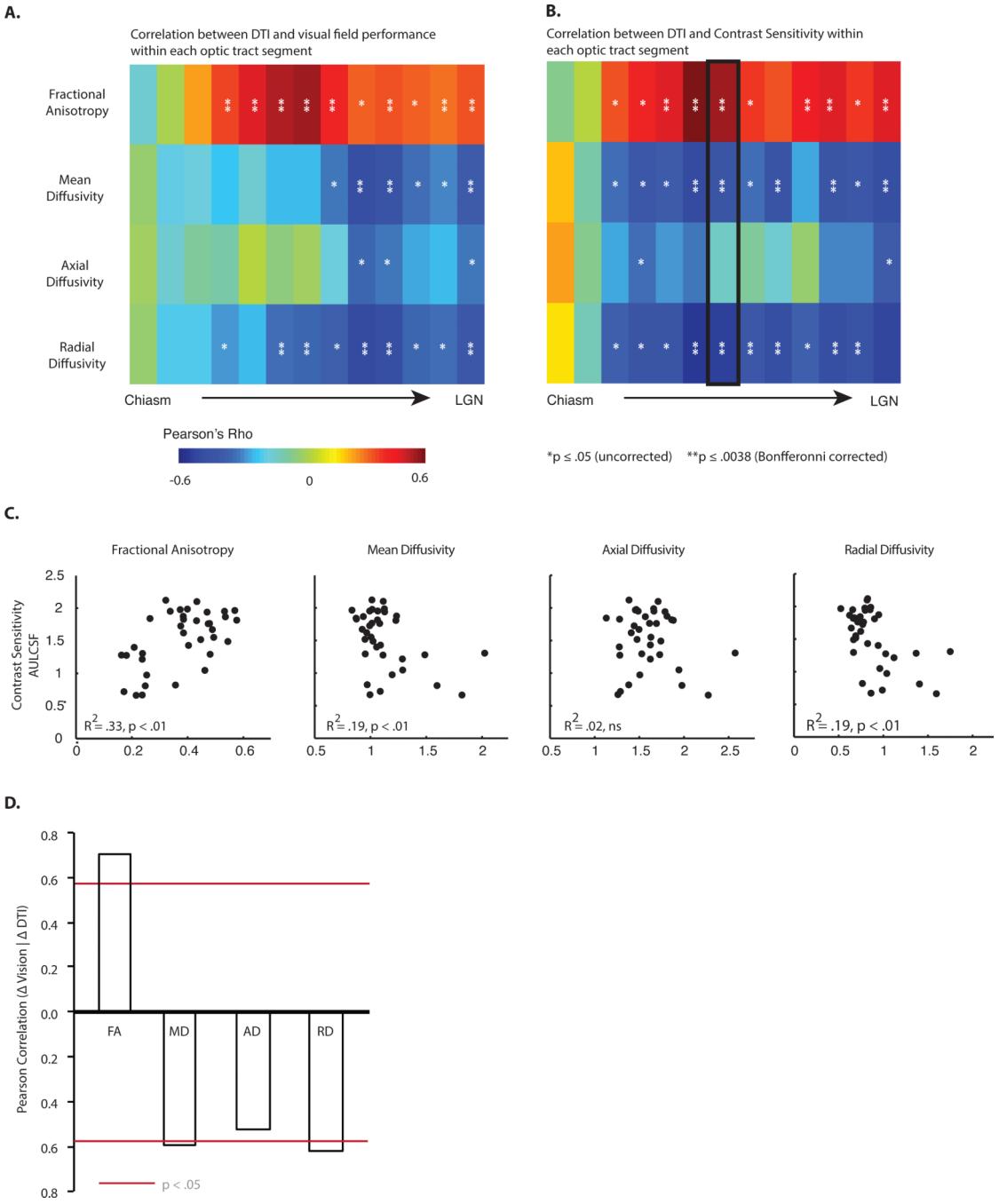

Figure 4. Relation between diffusion indices and visual ability

Within each segment of the optic tract, variability across all patients in diffusion indices was correlated with variability in **(A)** visual fields, and **(B)** AULCSF (area under the log contrast sensitivity function). Diffusion indices from a given optic tract (e.g., right) were correlated with psychophysical data from the contralateral visual field (e.g., left). While no relationships were observed between axial diffusivity and visual ability, radial diffusivity was negatively correlated with visual abilities. Near the optic chiasm (i.e. the first two segments), correlations were consistently poor for all diffusion indices, likely due to artifacts

from crossing retinofugal axons at the chiasm (* $p < .05$, uncorrected, ** $p < .0083$, Bonferroni corrected). **(C)** Diffusivity values from the middle segment of the optic tract (segment 7) are plotted against AULCSF. **(D)** A summary of the correlation between the change in diffusivity measurements in the optic tract and the change in visual abilities, as a function of surgery.

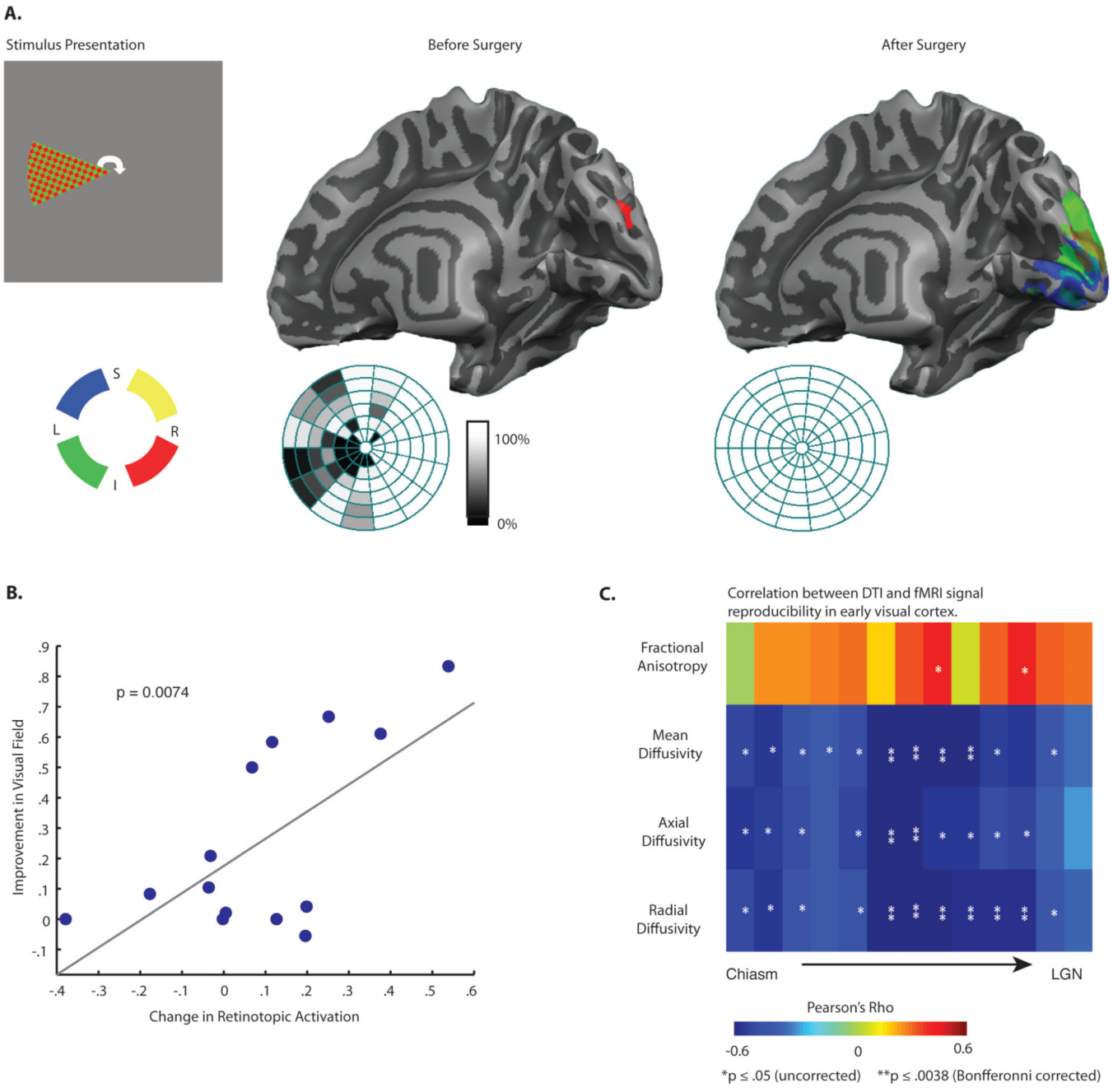

Figure 5. Relation among DTI, visual fields and retinotopic activity

(A) Example of visual field representations in early visual cortex in a single compressive pituitary tumor patient before and after surgery. Cortical responses in the right hemisphere normalized after surgery, while before surgery the only activation is a small spot of ectopic activity from the ipsilateral stimulus. Also shown are the same individual's visual fields for the left eye (right eye patched during scanning). (**B**) The scatter plot shows the effect of surgical decompression of the early visual pathway on visual fields and retinotopic activity, for corresponding quadrants—see text and Materials and Methods for details. (**C**) The relationships between diffusion indices for each segment of the optic tract and retinotopic

information content, displayed as a matrix of r-values (* $p < .05$, uncorrected, ** $p < .0083$, Bonferroni corrected).

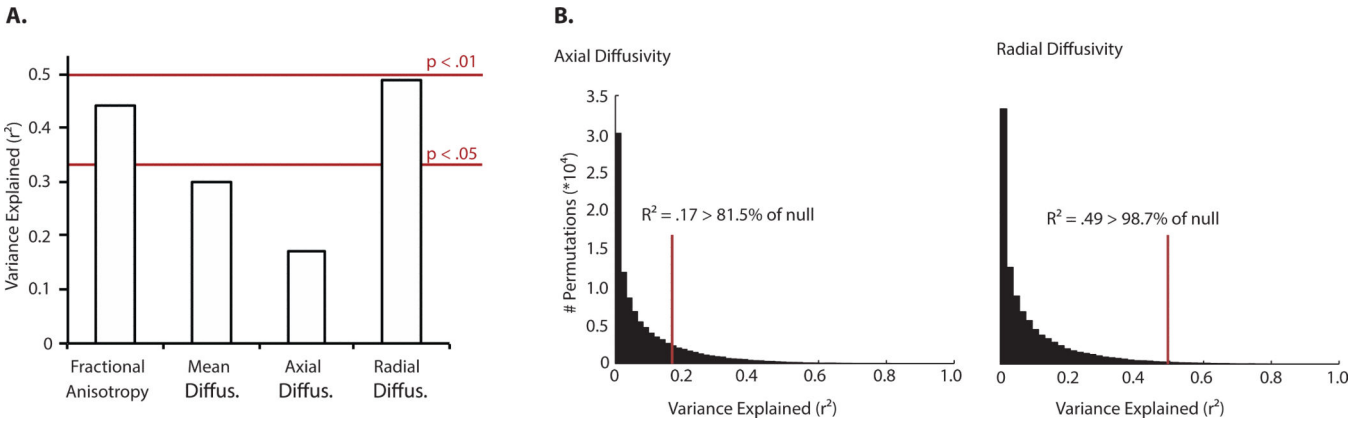

Figure 6. Pre-operative diffusivity along the optic tract predicts visual recovery

A support vector regression (SVR, linear kernel) model was trained on the along-tract diffusivity indices, separately for each of the four diffusivity measurements (fractional anisotropy - FA, mean diffusivity - MD, axial diffusivity - AD, and radial diffusivity – RD). The support vectors were trained on 11 hemispheres, and then tested on the 12th hemisphere. The analysis was jackknifed across the 12 hemispheres, each time leaving one out for test and training on the remaining 11. **(A)**. The graph plots explained variance in visual recovery across all hemispheres in the sample; while support vectors trained on along-tract measurements of radial diffusivity could predict 49% of the variance in the observed data, equivalent analyses with axial diffusivity predicted (a non-significant) 17% of the variance. **(B)**. Null distributions were bootstrapped using permutation tests over randomly shuffled data; histograms plot explained variance (r squared), for permutations over axial and radial diffusivity data. The vertical red line indicates the performance of the model on un-shuffled data (from panel A), and written percentages indicate where model performance fell along the bootstrapped null distribution.